

Pairwise interactions in inertially-driven one-dimensional microfluidic crystals

Kaitlyn Hood^{1,*} and Marcus Roper²

¹*Department of Mechanical Engineering, Massachusetts Institute of Technology, Cambridge, MA 02139, USA*

²*Department of Mathematics, University of California Los Angeles, Los Angeles, CA 90095, USA*

(Dated: September 11, 2022)

In microfluidic devices, inertia drives particles to focus on a finite number of inertial focusing streamlines. Particles on the same streamline interact to form one-dimensional microfluidic crystals (or “particle trains”). Here we develop an asymptotic theory to describe the pairwise interactions underlying the formation of a 1D crystal. Surprisingly, we show that particles assemble into stable equilibria, analogous to the motion of a damped spring. Although previously it has been assumed that particle spacings scale with particle diameters, we show that the equilibrium spacing of particles depends on the distance between the inertial focusing streamline and the nearest channel wall, and therefore can be controlled by tuning the particle radius.

In hydrodynamics, viscosity arises from collisions between the molecules of the fluid, transferring momentum from fast regions to slower regions. As a result, viscosity resists large velocity gradients, and is often compared to frictional damping. In contrast, fluid inertia maintains momentum and enhances velocity gradients in the flow. Heuristically, viscosity is thought to impede or dampen flow while inertia is thought to maintain it. Here we present a counterexample to this intuition. The geometry of the proposed system reverses the role of viscosity and inertia: viscous stresses perpetuate motion while inertial stresses dampen motion.

We consider the motion of two neutrally-buoyant particles suspended in a fluid moving through a rectangular channel. The Reynolds number of the flow is chosen between 1 and 100, so that inertial stresses are equal to or greater than viscous stresses. The fluid inertia causes the particles to migrate across streamlines and focus at finitely many inertial focusing streamlines [1–4]. Experiments [5–9] show that inertially focused particles “crystallize” into trains with regular spacing (Figure 1A-B).

There are two types of crystallization in rectangular microchannels for consideration: (i) cross-streamline crystals (which can be 2D or 3D) shown in Figure 1B and (ii) same-streamline crystals (effectively 1D crystals) shown in Figure 1A. Real particle trains are typically made up of a mixture of the two types [8]. Nonetheless, the two types of crystals have been explained by different mechanisms.

In case (i), lattice Boltzmann simulations [6] of the streamlines around a single inertially-focused particle showed the existence of two vortices on the opposite side of the channel (Figure 1C reproduces these). It was hypothesized that the centers of these vortices present stable focusing positions for a second particle. A stable crystal forms with particles alternating between streamlines.

In case(ii) crystalization is assumed to occur at the balance of attractive and repulsive inter-particle forces. The repulsive forces appear to be symmetric, while the attractive forces appear to be non-symmetric, and there-

fore are believed to have separate origins [7]. Lee *et al.* hypothesize that the repulsive forces are not due to fluid inertia – but rather are due to viscous interactions with the channel wall pushing the particles away from the focusing streamline. They assert that the attractive force arises from the inertial lift force pushing the particles back to their focusing streamlines and overshooting, creating a harmonic oscillator type potential.

While this mechanism gives a qualitative exploration of crystallization, it remains untested and generates more questions about the dynamics of train formation: What are the magnitudes of the attractive and repulsive forces? How do these forces depend on the experimental parameters? Can we predict the lattice length λ as a function of the experimental parameters? While general trends are well documented, and numerical simulations can predict dynamics for a single device, there is no theoretical model that can predict the lattice length for a general class of devices and range of parameters. Such a theory could be used to engineer trains with a specific lattice length. We analyze the interactions of pairs of particles confirming that pairs can form stable doublets in both cross-stream and same-streamline configurations. In the process of deriving this equilibrium spacing length between two particles we discover that these stable equilibria behave like simple damped spring models but that viscosity and inertia play unintuitive roles in the dynamics of these springs.

CROSS-STREAMLINE PAIRS

First we explore the mechanism by which particles interact across streamlines. We demonstrate mathematically how the center of a closed vortex can become a stable focusing position for a particle. Simulations [6] of the flow around a single inertially-focused particle show closed vortices on the opposite side of the channel (reproduced in Figure 1C). We assume that the original particle is on the focusing streamline $(y, z) = (h_1, 0)$ and the vortices are near the focusing streamline $(y, z) = (h_2, 0)$.

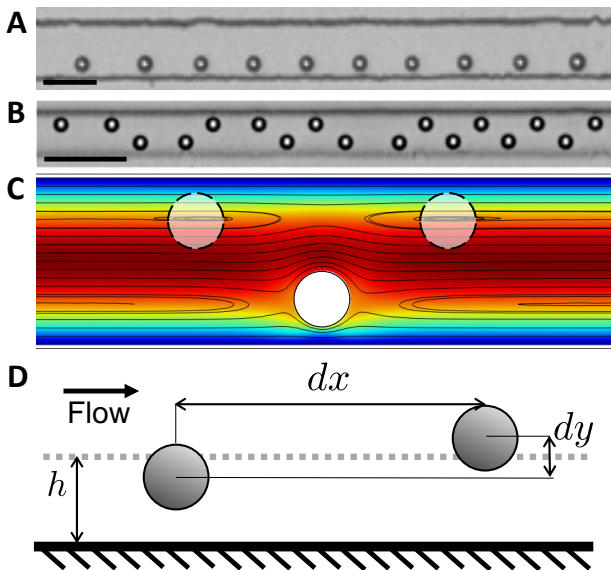


FIG. 1. (A) Particles on the same streamline form 1D microfluidic crystal for $Re = 30$ and $\alpha = 0.17$ and $AR = 1.7$, scale bar represents $90\mu\text{m}$ [8]. (B) Cross-streamline 2D microfluidic crystal, scale bar represents $50\mu\text{m}$ [7]. (C) Streamlines around a single inertially-focused particle simulated using FEM in Comsol Multiphysics (Los Angeles, CA) show stagnation points on the opposite side of the channel where particles can focus to form a stable crystal with particles alternating between streamlines. (D) Diagram for two particles near the inertial focusing streamline and a single wall.

Due to symmetry of the channel and inertial focusing, we will assume all particles are restricted to the plane $z = 0$. Initially we treat the eddies phenomenologically; but we note that the eddies themselves can be quantitatively reproduced using the same model we develop for same streamline interactions (See the Supplemental Material).

For simplicity, we assume the closed vortex has an elliptical shape in the x, y -plane and is centered at (x_c, y_c) , where y_c is sufficiently close to h_2 . Then we can express the vortex as a second order system of ODEs:

$$\dot{x} = -\beta^2(y - y_c), \quad \dot{y} = \omega^2(x - x_c). \quad (1)$$

Now we consider a second particle near the h_2 streamline. The particle has an inertial migration velocity [10] which can be expressed as $\dot{y} = -\Gamma(y - h_2)$, where:

$$\Gamma = \frac{a^3 U Re}{6\pi H^4} \left(95.9 + 163.4 \frac{a}{H} \right). \quad (2)$$

To add inertial focusing to the system of ODEs above, we make the change of variables $X = x - x_c$ and $Y = y - y^*$, where we will determine the value of y^* later on. Then we rewrite the ODEs as:

$$\dot{X} = -\beta^2(Y + y^* - y_c), \quad (3)$$

$$\dot{Y} = \omega^2 X - \Gamma(Y - y^* - h_2). \quad (4)$$

By substitution we can re-write this as a second-order ODE in Y :

$$\ddot{Y} + \Gamma\dot{Y} + \omega^2\beta^2 Y = -\omega^2\beta^2(y^* - y_c) - \Gamma(y^* - h_2). \quad (5)$$

The right hand side of equation (5) equal to zero if we choose y^* to be:

$$y^* = \frac{\omega^2\beta^2 y_c + \Gamma h_2}{\omega^2\beta^2 + \Gamma}. \quad (6)$$

Then equation (5) becomes a homogeneous second-order differential equation with constant coefficients, or a damped harmonic oscillator. We see that the damping term is proportional to Γ , the inertial focusing constant. As a result, the particle focuses to $(X, Y) = (0, 0)$ or $(x, y) = (x_c, y^*)$.

We have shown that the damping of particle motion in an eddy due to inertial focusing forces the particle to focus to a single point. Notice that the focusing position of the particle is not exactly on the inertial-focusing streamline, but at a weighted average between the streamline and the center of the eddy, where the weights are the inertial focusing constant Γ and the elliptical eddy constants β and ω .

This analysis provides a mechanism by which particles can form stable cross-stream pairs. However, it does not appear to apply to same-streamline crystals because there are no closed eddies on the same streamline as the focused particle, only a recirculating flow (Figure 1C). In order to explain same-streamline crystallization, we need to derive a new model from first principles.

SAME-STREAMLINE PAIRS

Here we derive a model for the assembly of pairs of same-streamline crystals. Consider fluid flowing through a rectangular channel with height H , width W , and aspect ratio $AR = W/H$, and fluid flowing with maximum velocity U . If the fluid has density ρ and viscosity μ then the channel Reynolds number is $Re = \rho U H / \mu$. We consider two spherical particles with radius a and density ρ suspended in the fluid, both close to a given inertial focusing streamline. The distance h between the inertial focusing streamline and the channel wall can be predicted from asymptotic theory [11] and is a function of the relative particle-to-channel size $\alpha = a/H$. Let dx be the downstream separation of the two particles (from center to center) and dy be the vertical displacement of the downstream particle above the upstream particle (Figure 1D). In order to make an asymptotic expansion, we assume that $a \ll h \ll dx$.

Because of the no-slip boundary condition on the walls of the channel, the fluid velocity \mathbf{u} cannot grow to be too large, and therefore neither can the fluid inertia [11]. Hence, a three-dimensional asymptotic analysis of the

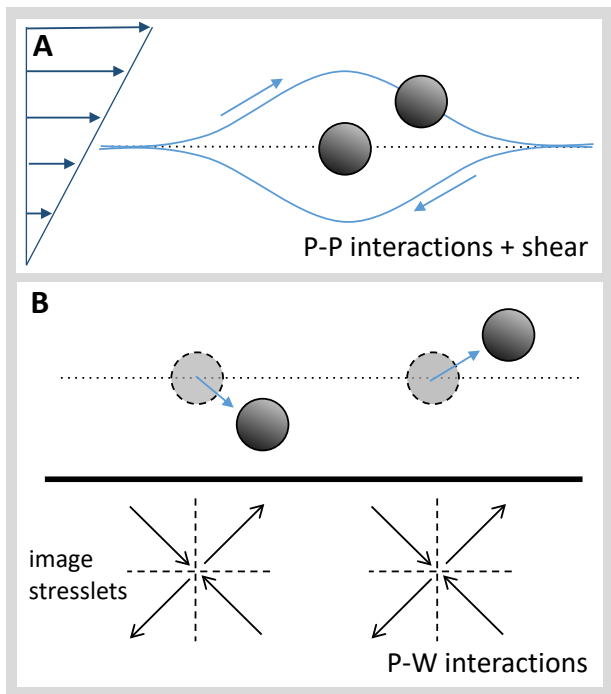


FIG. 2. (A) Viscous P-P interactions with shear predicts that two particles starting on the same streamline endlessly orbit each other with $\dot{d}y < 0$. Shown in the moving reference frame of one particle. (B) Viscous P-W interactions can be represented by image stresslets. The image on particle 1 acts on particle 2 and vice versa, creating a net $\dot{d}y > 0$.

Navier-Stokes equations for this system showed that a low Reynolds number approximation is valid throughout the channel [11]. This analysis demonstrated that the dominant physics is viscous, and that inertial focusing can be treated as a perturbative effect.

What are the minimal physics needed to model the interactions of a pair of particles within a same-streamline 1D crystal? First, we need inertial focusing to constrain the particles on a streamline. Second, we need particle-particle (P-P) interactions. Third we need the local background flow (i.e. the flow in a channel undisturbed by particles), which to first order is a shear flow. Fourth, we find that it is necessary to include particle-wall (P-W) interactions (with the nearest channel wall) in order to achieve a stable configuration. The role of the P-W interactions will be made clear later in this section.

It suffices to approximate the P-P interactions and the P-W interactions with their viscous counterparts since the asymptotic theory shows that, in a channel geometry, viscous effects are first order and inertial effects are second order [11]. Furthermore, these viscous interactions can be written analytically as a multipole expansion. Likewise, inertial focusing can be written as a two-term asymptotic series whose coefficients were computed numerically by Hood *et al.* [11].

Viscous P-P interactions in a shear flow can be ex-

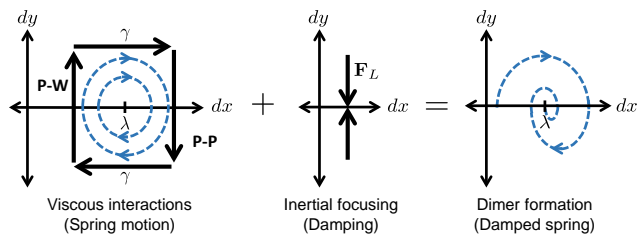


FIG. 3. Analogy between nucleation and damped spring motion.

pressed by multipole expansion [12, 13]. Two particles starting on the same streamline endlessly orbit each other (Figure 2A). Because this orbit is clockwise in the sense of the coordinates used in Figure 1D and 2A, $\dot{d}y$ is negative throughout.

Viscous P-W interactions act in the opposite direction on the vertical displacement dy . We can see this by using the method of images to model the effect of the wall on the particles. To first order, we approximate the image particles by stresslets. The induced velocity on the downstream particle is calculated by evaluating the upstream image stresslet at the center of the downstream particle and has a positive y component. Likewise the induced velocity on the upstream component has a negative y component, so that the net vertical displacement $\dot{d}y$ is positive (Figure 2B).

The shear flow centered at the height h turns any vertical displacement dy into a downstream displacement dx . Combining the shear flow with viscous P-P interactions and viscous P-W interactions creates a closed loop with an equilibrium point at $(dx, dy) = (\lambda, 0)$ (Figure 3 left). In dynamical systems, $(\lambda, 0)$ is called a center and is neutrally stable. Note that when the particles are on the same streamline, neither P-P nor P-W interactions act to alter the spacing dx directly. The equilibrium shows up as a point where $\dot{d}y$ vanishes. Thus, it is not detected using the standard approach to finding equilibria (i.e. analyzing where $\dot{d}x = 0$).

In contrast, inertial focusing acts uniformly on particles, regardless of their separation dx , and always pushes particles back to the inertial focusing streamline at $y = h$. Therefore inertial focusing pushes $\dot{d}y$ to zero (Figure 3 center). Adding inertial focusing to the viscous system above creates an asymptotically stable spiral point that converges to $(dx, dy) = (\lambda, 0)$ (Figure 3 right).

The dynamics of the system of two inertially-focused particles interacting mimics the behavior of a damped harmonic oscillator or a spring with frictional damping (Figure 3). Here the viscous interactions are analogous to the spring motion creating closed trajectories in (dx, dy) space while inertial focusing is analogous to frictional damping. Herein lies the role-reversal: viscosity maintains motion (like a spring) and inertia dampens motion (like friction).

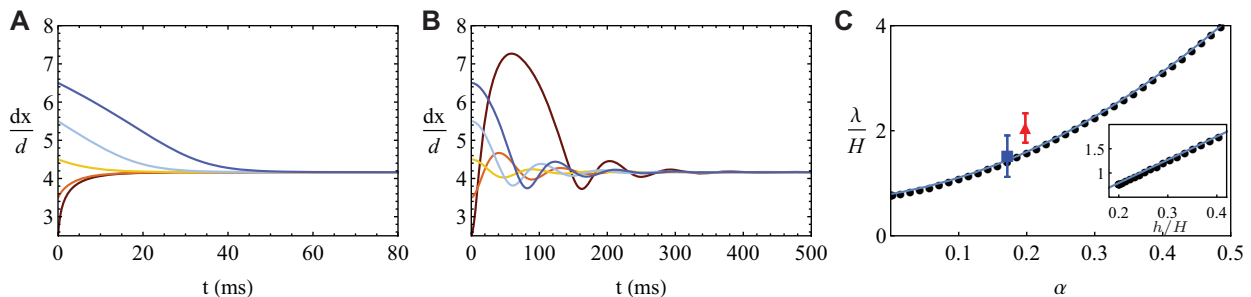


FIG. 4. The separation of two particles $dx(t)$ as a function of time for $a = 6\mu\text{m}$, different initial separation lengths, and (A) $Re = 30$ or (B) $Re = 1$. (C) The equilibrium separation length λ is a function of the relative particle size α matches equation (12). Here the markers represent numerical solutions to equations (9)-(10) and the solid line is equation (12). Experimental measurements from Kahkeshani *et al.* [8] at $Re_p = 2.8$ (blue square) and Lee *et al.* [7] (red triangle) agree with our model. Error bars are standard deviations. (Inset) We observe that λ is a linear function of h and can be approximated by equation (11).

DYNAMIC MODEL OF CRYSTALLIZATION

We can make this description rigorous by writing down the equations of motion and solving them numerically. Let \mathbf{x}_i for $i = 1, 2$ be the locations of the two particles. The flow around each particle can be derived using the Lamb's solution for the flow exterior to a sphere [14, 15]. Here we will only keep the terms that are $O(r^{-2})$ and $O(r^{-3})$. In order to derive the image system in the next step, we must convert the Lamb's solution into multipole singularities. In this case the $O(r^{-2})$ term becomes the stresslet \mathbf{v}^{ST} , and the $O(r^{-3})$ term is decomposed into the source dipole \mathbf{v}^{D} and two stokeslet quadrupoles \mathbf{v}^{SQ} and \mathbf{w}^{SQ} . See Supplemental material at (link) for detailed derivation of these terms and their images below.

For each particle, we model the viscous wall effects by computing the image system for a plane wall. Blake [16] derived the image system for a stokeslet, and using a similar procedure the image systems for the stresslet \mathbf{v}^{STim} , source dipole \mathbf{v}^{Dim} , and stokeslet quadrupoles \mathbf{v}^{SQim} and \mathbf{w}^{SQim} can be derived [17, 18]. Then the flow around each particle is:

$$\mathbf{v}_i \sim (\mathbf{v}_i^{\text{ST}} + \mathbf{v}_i^{\text{STim}}) + (\mathbf{v}_i^{\text{D}} + \mathbf{v}_i^{\text{Dim}}) + (\mathbf{v}_i^{\text{SQ}} + \mathbf{v}_i^{\text{SQim}}) + (\mathbf{w}_i^{\text{SQ}} + \mathbf{w}_i^{\text{SQim}}). \quad (7)$$

Let $\bar{\mathbf{u}}$ be the Poiseuille flow through a rectangular channel [19]. Then, for each particle we can compute the induced velocity from the other particle and image system,

$$\mathbf{U}_i = \left(1 + \frac{a^2}{6} \nabla^2\right) (\bar{\mathbf{u}} + \mathbf{v}_j) \Big|_{\mathbf{x}=\mathbf{x}_i}, \quad i \neq j. \quad (8)$$

Then we define the relative velocity $d\mathbf{U} = \mathbf{U}_2 - \mathbf{U}_1$.

We again model inertial focusing by Taylor expanding the migration velocity from Hood *et al.* [10] in the coordinate y around h . This gives $\dot{y}_i = -\Gamma(y_i - h)$,

where the inertial focusing constant Γ is defined in equation (2). Combining the viscous particle interactions $d\mathbf{U} = (dU, dV, 0)$ with the inertial focusing we arrive at a system of ODEs for the dynamics of particle interactions:

$$\dot{dx} = dU, \quad dx(t=0) = k_0 d, \quad (9)$$

$$\dot{y}_i = V_i - \Gamma(y_i - h), \quad y_i(t=0) = h, \quad i = 1, 2. \quad (10)$$

The ODEs depend explicitly on the particle size α , the Reynolds number Re , and the initial separation length $k_0 d$. The equations implicitly depend on the channel aspect ratio AR , but throughout this paper we will consider the same channel as Kahkeshani *et al.* [8], where $W = 60\mu\text{m}$, $H = 35\mu\text{m}$, and $AR = 1.7$.

Solving ODEs (9)-(10) numerically for $Re = 30$, $a = 6\mu\text{m}$, and various initial conditions shows that there is a stable equilibrium length $\lambda = 4.15d$ (Figure 4A). In contrast, the same system for $Re = 1$ converges to the same value of $\lambda = 4.15d$, but the harmonic oscillator becomes under-damped (Figure 4B). This shows that as Re increases, so does the damping of the spring motion.

How does the lattice length λ scale with experimental parameters? Contrary to expectations, we find that λ does not scale simply with particle diameter $d = 2a$. From the derivation of our asymptotic model, we would expect λ to depend on both the particle radius a and the distance from the inertial-focusing streamline to the wall h . Surprisingly, we find from the numerical solutions of equations (9)-(10) that λ depends linearly on h (Figure 4C Inset). A polynomial fit of the numerical data predicts that:

$$\lambda = -0.2H + 4.8h. \quad (11)$$

We conjecture that h is the scaling parameter for the equilibrium spacing, instead of λ . It is not surprising that h influences λ strongly because h appears in the P-W interaction term, which was necessary to include in our

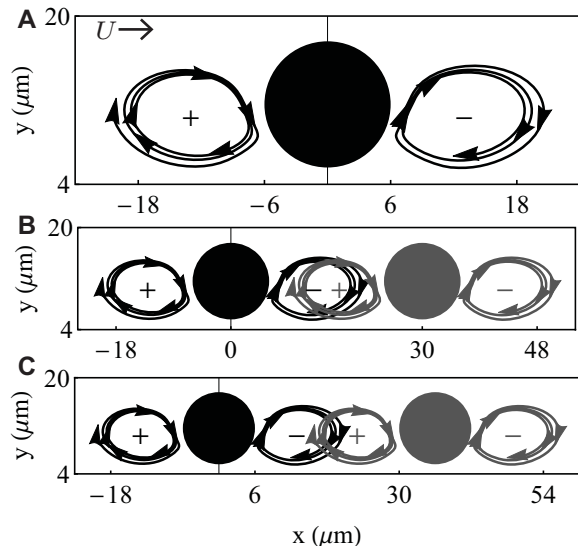


FIG. 5. (A) Streamlines for a particle on the inertial focusing streamline has two vortices. The trailing vortex spirals outward while the leading vortex spirals inward. (B) If particles approach too closely, then vortices interfere constructively. (C) If particles are spaced further apart, the vortices interfere destructively.

model in order to form stable equilibria. In terms of the qualitative model of Lee *et al.* [7], the P-P interactions give rise to a repulsive force between the particles while the P-W interactions lead to an attractive force. Since the strength of the P-W interactions depend explicitly on h , it follows that h should strongly determine the equilibrium spacing λ .

Additionally, h depends implicitly on the relative particle size $\alpha = a/H$ (recall that H is the height of the channel), and can be approximated by a quadratic polynomial [11]. Therefore, we expect that λ can be expressed as a function of the relative particle size α . Using a similar analysis, we observe that for infinitesimal particle sizes, the equilibrium spacing λ approaches a constant $\lambda \sim 0.8H$ (Figure 4C). As particle size α increases, λ also increases. A polynomial fit of the numerical data for λ predicts that:

$$\frac{\lambda}{H} = 0.8 + 2.2\alpha + 9.1\alpha^2. \quad (12)$$

We compare the numerical data and the numerical fit in equation (12) to experimental data from Kahkeshani *et al.* [8] (at $Re_p = 2.8$) and Lee *et al.* [7] (Figure 4C). We observe experimental measurements agree with our model with no fitting parameters, even though the channels have different aspect ratios ($AR = 1.7$ and $AR = 3.6$, respectively).

We note that the equilibrium spacing λ is independent of Re in our theory (though our theory is asymptotically correct as $Re \rightarrow 0$, so higher order corrections are needed to model the effect of Re on the equilibrium spacing). For

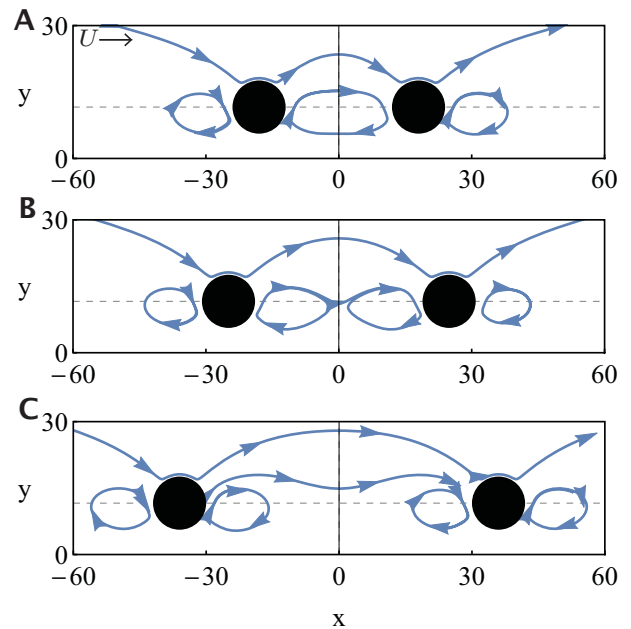


FIG. 6. Vortex interactions for two inertially-focused particles. (A) $dx = 3d < \lambda$, (B) $dx = 4.15d = \lambda$, (C) $dx = 6d > \lambda$.

our system, Re does not impact the equilibrium of the system, only the degree of damping.

A SCHEMATIC EXPLANATION FOR CRYSTALLIZATION AT MODERATE REYNOLDS NUMBERS

In our model, we assume particle interactions are dominated by viscosity; which is asymptotically correct in the limit of small Reynolds numbers. However, particle train formation still occurs at moderate Re , although Kahkeshani *et al.* showed preferred spacings of particles can change as Re increases [8].

As a first step toward a physical theory for crystallization at moderate Reynolds numbers, we adopt an approach recently used to study particle chaining in acoustic streaming flows [20, 21]. We analyze the vortical structures created by single particles and then look for patterns of interference between particles. Klotsa *et al.* find empirically that particles tend to organize themselves into configurations that minimize total kinetic energy in the surrounding flow [21].

We investigate the approximate velocity around a single inertially-focused particle \mathbf{U}_i . Note that the trajectories of $\mathbf{u}_i(\mathbf{x})$ show the paths that another particle would follow if introduced at a point \mathbf{x} ; they are therefore particle paths, not streamlines. As a result, they are not evident in simulations showing the directions of fluid flow (e.g. Figure 1C). We observe that the particle paths form a leading vortex and a trailing vortex both with the same sense of rotation (Figure 5). On closer observation we

notice that neither structure is closed. These zones of recirculation have been observed experimentally [8]. The leading vortex is an inward spiral, while the trailing vortex is an outward spiral (Figure 5). Closure (or not) of the eddies is not a significant factor in our following analysis.

When two particles are spaced far apart, their respective leading and trailing vortices will tend to cancel each other, as shown in the schematic in Figure 5C. However, if the particles are brought close enough together that the vortices overlap, then the vortices will reinforce each other, as shown in Figure 5B. No longer cancelling, the kinetic energy of the flow will now increase. Following the reasoning of Klotsa *et al.* [21], we expect the particles to self-organize into a configuration that minimizes the kinetic energy, i.e. intermediate between Figures 5B and 5C.

We confirmed that these predictions are supported in our simulations of particles interacting at small Reynolds numbers. When the two particles are close together, $dx < \lambda$, then the two vortices combine to form a closed ring (Figure 6A). When the particles are too far apart $dx > \lambda$, the vortices cancel only weakly (Figure 6C). Conversely, when the particles are at their equilibrium spacing $dx = \lambda$, the vortices connect to each other but maintain their distinct centers (Figure 6B).

CONCLUSIONS

Under our model, pairs of particles organize into stable equilibria that are analogous to damped springs, in which the expected roles of inertia and viscosity have been reversed. Viscous flow maintains harmonic motion, like a spring, while inertial focusing results in a damping effect.

The minimal physics needed to model the harmonic motion are: shear flow, particle-particle interactions and particle-wall interaction. We showed that particle-wall interactions are necessary to achieve negative vertical displacement dy , and therefore necessary to achieve closed trajectories in the viscous harmonic motion.

We developed an asymptotic model to describe this behavior and produced a formula for the lattice spacing λ . We envisage that the model for particle spacing (the terms of which are directly written out in the Supplementary Material) will be generally useful for reduced order simulations for particles in inertial microfluidic devices. We showed that λ scales with the distance h between the inertial focusing streamline and the channel wall. Since the distance h depends on the relative particle size $\alpha = a/H$, the lattice spacing λ can be tuned by changing particle sizes. As a result, not only is the effect

of the channel walls necessary to model the dynamics, but it also sets the scaling for the lattice length.

ACKNOWLEDGMENTS

This material is based upon work supported by the National Science Foundation under Award No. DMS-1606487 (to K.H.) and DMS-1312543 (to M.R.). This work was partially supported by the UCLA Dissertation Year Fellowship (to K.H.). We thank Lawrence Liu for performing preliminary simulations (supported by DMS-1045536), and Hamed Haddadi and Soroush Kahkeshani for helpful discussions.

* kaitlyn.t.hood@gmail.com

- [1] G. Segré and A. Silberberg, *Nature* **189**, 209 (1961).
- [2] D. Di Carlo, D. Irimia, R. G. Tompkins, and M. Toner, *Proc. Natl. Acad. Sci.* **104**, 18892 (2007).
- [3] D. Di Carlo, J. F. Edd, K. J. Humphry, H. A. Stone, and M. Toner, *Phys. Rev. Lett.* **102**, 094503 (2009).
- [4] Y.-S. Choi, K.-W. Seo, and S.-J. Lee, *Lab chip* **11**, 460 (2011).
- [5] J.-P. Matas, V. Glezer, É. Guazzelli, and J. F. Morris, *Phys. Fluids* (1994-present) **16**, 4192 (2004).
- [6] K. J. Humphry, P. M. Kulkarni, D. A. Weitz, J. F. Morris, and H. A. Stone, *Phys. Fluids* **22**, 081703 (2010).
- [7] W. Lee, H. Amini, H. A. Stone, and D. Di Carlo, *Proc. Natl. Acad. Sci.* **107**, 22413 (2010).
- [8] S. Kahkeshani, H. Haddadi, and D. Di Carlo, *J. Fluid Mech.* **786**, R3 (2016).
- [9] A. E. Reece and J. Oakey, *Phys. Fluids* (1994-present) **28**, 043303 (2016).
- [10] K. Hood, S. Kahkeshani, D. Di Carlo, and M. Roper, *Lab Chip* **16**, 2840 (2016).
- [11] K. Hood, S. Lee, and M. Roper, *J. Fluid Mech.* **765**, 452 (2015).
- [12] G. Batchelor and J.-T. Green, *J. Fluid Mech.* **56**, 375 (1972).
- [13] F. Da Cunha and E. Hinch, *J. Fluid Mech.* **309**, 211 (1996).
- [14] H. Lamb, *Hydrodynamics* (Dover Publications, 1945).
- [15] S. Kim and S. Karrila, *Microhydrodynamics: Principles and Selected Applications*, Butterworth - Heinemann series in chemical engineering (Dover Publications, 2005).
- [16] J. Blake, in *Math. Proc. Cambridge Philos. Soc.*, Vol. 70 (Cambridge Univ Press, 1971) pp. 303–310.
- [17] J. Blake and A. Chwang, *J. Eng. Math.* **8**, 23 (1974).
- [18] S. E. Spagnolie and E. Lauga, *J. Fluid Mech.* **700**, 105 (2012).
- [19] T. C. Papanastasiou, G. C. Georgiou, and A. N. Alexandrou, *Viscous Fluid Flow* (CRC Press, 1999).
- [20] D. Klotsa, M. R. Swift, R. Bowley, and P. King, *Physical Review E* **76**, 056314 (2007).
- [21] D. Klotsa, M. R. Swift, R. Bowley, and P. King, *Physical Review E* **79**, 021302 (2009).
- [22] L. Chow, J. Leland, J. Beam, and E. Mahefkey, *Journal of fluids engineering* **111**, 229 (1989).

Supplemental Materials: Nucleation of inertially-driven one-dimensional microfluidic crystals

Kaitlyn Hood and Marcus Roper

DERIVATION OF THE VISCOUS MODEL FOR TWO PARTICLES

Here we derive an asymptotic model of two particles in a Poiseuille flow near a wall. We use this model to predict the equilibrium spacing of two particles in an inertial microfluidic device. We compare our asymptotic model to numerical simulations of the full Navier-Stokes equation, themselves fully validated in section .

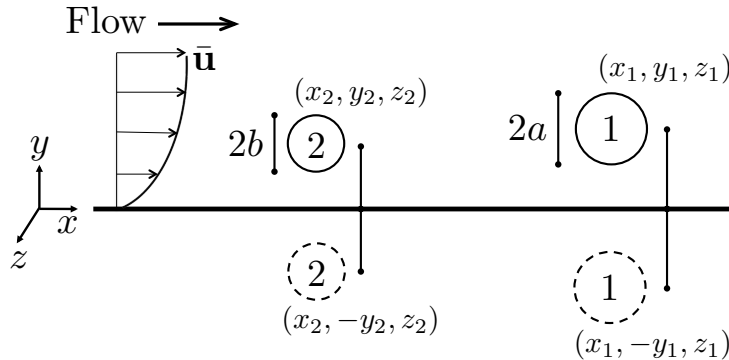


FIG. S1. Two particles near a wall at $y = 0$ in a parabolic background flow $\bar{\mathbf{u}}$. The particles have radius a and b respectively, and are located at positions (x_1, y_1, z_1) and (x_2, y_2, z_2) .

We consider the flow around two particles near a wall. The particles have radius a and b , respectively, and the wall is located at $y = 0$. The particles are centered at (x_i, y_i, z_i) for $i = 1, 2$ and have image systems centered at the reflection point across the wall $(x_i, -y_i, z_i)$ (Figure S1).

We will derive this model for arbitrary parameters a , b , x_i , y_i , and z_i for $i = 1, 2$ which satisfy the following assumptions:

$$z_1 - z_2 \ll a, b \ll y_1, y_2 \ll x_1 - x_2. \quad (\text{S1})$$

Once we have the model, in order to compare to experimental data, we will make the following substitutions:

$$z_1 = z_2 = 0, \quad a = b, \quad y_1 = y_2 = h, \quad \text{and} \quad dx = x_1 - x_2. \quad (\text{S2})$$

The objective is to find the separation length dx for which the particles have no relative motion.

Flow around a single particle in the background flow.

The background flow in a rectangular channel is the Poiseuille flow [S19]. Here we will approximate this flow by its Taylor expansion in the coordinate y ,

$$\bar{\mathbf{u}} \sim \beta + \gamma_y(y - y_i) + \delta_{yy}(y - y_i)^2. \quad (\text{S3})$$

The flow around the particle can be derived using the Lamb's solution for the flow exterior to a sphere [S14, S15]. Here we will only keep the term that are $O(r^{-2})$ and $O(r^{-3})$. In order to derive the image system in the next step, we must convert the Lamb's solution into multipole singularities. In this case the $O(r^{-2})$ term becomes the stresslet, and the $O(r^{-3})$ term is decomposed into the source dipole \mathbf{v}^D and two stokeslet quadrupoles \mathbf{v}^{SQ} and \mathbf{w}^{SQ} . Define

$\mathbf{r}_i = (x - x_i, y - y_i, z - z_i)$ and $r_i = |\mathbf{r}_i|$, then the flow $\mathbf{v}_i^0 \sim \mathbf{v}_i^{\text{ST}} + \mathbf{v}_i^{\text{D}} + \mathbf{v}_i^{\text{SQ}} + \mathbf{w}_i^{\text{SQ}}$ around each particle satisfies

$$\mathbf{v}_i^{\text{ST}} = -\frac{5\gamma_y}{2} \left[\frac{(x - x_i)(y - y_i)}{r_i^3} \mathbf{r}_i \right] \frac{1}{r_i^2}, \quad \mathbf{v}_i^{\text{D}} = -\frac{7\delta_{yy}}{24} \left[\mathbf{e}_x - \frac{3(x - x_i)}{r_i^2} \mathbf{r}_i \right] \frac{1}{r_i^3}, \quad (\text{S4})$$

$$\mathbf{v}_i^{\text{SQ}} = -\frac{\delta_{yy}}{12} \left[\mathbf{e}_x - \frac{3(y - y_i)^2}{r_i^2} \mathbf{e}_x - \frac{3(x - x_i)}{r_i^2} \mathbf{r}_i + \frac{15(x - x_i)(y - y_i)^2}{r_i^4} \mathbf{r}_i \right] \frac{1}{r_i^3}, \quad (\text{S5})$$

$$\mathbf{w}_i^{\text{SQ}} = -\frac{5\delta_{yy}}{24} \left[-\mathbf{e}_x + \frac{3(y - y_i)^2}{r_i^2} \mathbf{e}_x - \frac{6(x - x_i)(y - y_i)}{r_i^2} \mathbf{e}_y - \frac{3(x - x_i)}{r_i^2} \mathbf{r}_i + \frac{15(x - x_i)(y - y_i)^2}{r_i^4} \mathbf{r}_i \right] \frac{1}{r_i^3}. \quad (\text{S6})$$

Image system for each particle due to the wall.

Blake derived the image system for a stokeslet [S16]. Using a similar procedure we derive the image systems for a stresslet and a source dipole. Define $\mathbf{R}_i = (x - x_i, y + y_i, z - z_i)$ and $R_i = |\mathbf{R}_i|$.

The image system for the stresslet is:

$$\mathbf{v}_i^{\text{STim}} = \left[\frac{(x - x_i)(y + y_i)}{2R_i^3} \mathbf{R}_i - \frac{5yy_i(x - x_i)(y + y_i)}{R_i^5} \mathbf{R}_i + \frac{yy_i(y + y_i)}{R_i^3} \mathbf{e}_x - \frac{y_i^2(x - x_i)}{R_i^3} \mathbf{e}_y \right] \frac{5\gamma_y}{R_i^2} \quad (\text{S7})$$

The image system for the source dipole is:

$$\mathbf{v}_i^{\text{Dim}} = \frac{\delta_{yy}}{4} \left[\frac{30y(y + y_i)}{R_i^4} \mathbf{R}_i - \frac{3(3y + y_i)}{R_i^2} \mathbf{R}_i - \frac{6(y^2 - y_i^2)}{R_i^2} \mathbf{e}_y - \mathbf{e}_y \right] \frac{1}{R_i^3} \quad (\text{S8})$$

The image system for the first stokeslet quadrupole is:

$$\mathbf{v}_i^{\text{SQim}} = -\frac{\delta_{yy}}{24} \left[\frac{3(x - x_i)}{R_i^2} \mathbf{R}_i - \frac{15(x - x_i)(y + y_i)^2}{R_i^4} \mathbf{R}_i - \frac{30yy_i(x - x_i)}{R_i^4} \mathbf{R}_i + \frac{210yy_i(x - x_i)(y + y_i)^2}{R_i^6} \mathbf{R}_i \right. \\ \left. - \frac{30y_i(x - x_i)(y^2 - y_i^2)}{R_i^4} \mathbf{e}_y - \frac{6y_i(x - x_i)}{R_i^2} \mathbf{e}_y - \frac{30yy_i(y + y_i)^2}{R_i^4} \mathbf{e}_x + \frac{3(y + y_i)^2}{R_i^2} \mathbf{e}_x + \frac{6yy_i}{R_i^2} \mathbf{e}_x - \mathbf{e}_x \right] \frac{1}{R_i^3}. \quad (\text{S9})$$

The image system for the second stokeslet quadrupole is:

$$\mathbf{w}_i^{\text{SQim}} = -\frac{5\delta_{yy}}{24} \left[\frac{3(x - x_i)}{R_i^2} \mathbf{R}_i - \frac{15(x - x_i)(y + y_i)^2}{R_i^4} \mathbf{R}_i - \frac{30(x - x_i)(2y + 3y_i)}{R_i^4} \mathbf{R}_i \right. \\ \left. + \frac{210yy_i(x - x_i)(y + y_i)^2}{R_i^6} \mathbf{R}_i - \frac{30y_i(x - x_i)(y^2 - y_i^2)}{R_i^4} \mathbf{e}_y - \frac{3(y + y_i)^2}{R_i^2} \mathbf{e}_x \right. \\ \left. + \frac{6(x - x_i)(y - 2y_i)}{R_i^2} \mathbf{e}_y + \frac{6y(2y + 3y_i)}{R_i^2} \mathbf{e}_x - \frac{30yy_i(y + y_i)^2}{R_i^4} \mathbf{e}_x + \mathbf{e}_x \right] \frac{1}{R_i^2}. \quad (\text{S10})$$

Induced velocities from particle and image system.

Up to this point we have derived the flow around each particle due to the background flow and the wall,

$$\mathbf{v}_i \sim (\mathbf{v}_i^{\text{ST}} + \mathbf{v}_i^{\text{STim}}) + (\mathbf{v}_i^{\text{D}} + \mathbf{v}_i^{\text{Dim}}) + (\mathbf{v}_i^{\text{SQ}} + \mathbf{v}_i^{\text{SQim}}) + (\mathbf{w}_i^{\text{SQ}} + \mathbf{w}_i^{\text{SQim}}). \quad (\text{S11})$$

For each particle we can compute the induced velocity from the other particle and image system,

$$\mathbf{U}_1 = \left(1 + \frac{a^2}{6} \nabla^2 \right) (\bar{\mathbf{u}} + \mathbf{v}_2) \Big|_{\mathbf{x}=\mathbf{x}_1}, \quad \mathbf{U}_2 = \left(1 + \frac{b^2}{6} \nabla^2 \right) (\bar{\mathbf{u}} + \mathbf{v}_1) \Big|_{\mathbf{x}=\mathbf{x}_2}. \quad (\text{S12})$$

Then we define the relative velocity $d\mathbf{U} = \mathbf{U}_2 - \mathbf{U}_1$. The particles are considered to be in equilibrium when their induced velocities are equal, that is $d\mathbf{U} = 0$.

The separation length for two particles.

Now we want to find the separation length for two particles. We are going to assume that the particles are the same size and are already inertially focused, that is:

$$a = b, \quad y_1 = y_2 = h, \quad z_1 = z_2 = 0. \quad (\text{S13})$$

Then we define the separation length as $dx = x_1 - x_2$. The objective is to find dx for which $d\mathbf{U} = 0$.

Define $r^2 = (x_1 - x_2)^2 + (y_1 - y_2)^2 + (z_1 - z_2)^2 = dx^2$ and $R^2 = (x_1 - x_2)^2 + (y_1 + y_2)^2 + (z_1 - z_2)^2 = dx^2 + 4h^2$. Let $d\mathbf{U} = (dU, dV, dW)$, then each component satisfies:

$$dU = -\frac{10\gamma_y h dx^2 (dx^2 + 5h^2)}{3(dx^2 + 4h^2)^{7/2}}, \quad (\text{S14})$$

$$dV = -\frac{5\gamma_y a^2}{3dx^4} + \frac{10h^2\gamma_y dx(dx^4 - 12h^2dx^2 - 64h^4)}{(dx^2 + 4h^2)^{9/2}} + \frac{5a^2\gamma_y dx(dx^4 - 72h^2dx^2 + 256h^4)}{3(dx^2 + 4h^2)^{9/2}} \quad (\text{S15})$$

$$+ \frac{5h^3\delta_{yy} dx(27dx^4 + 20h^2dx^2 - 352h^4)}{(dx^2 + 4h^2)^{11/2}} + \frac{10ha^2\delta_{yy} dx(15dx^4 - 265h^2dx^2 + 464h^4)}{3(dx^2 + 4h^2)^{11/2}},$$

$$dW = 0. \quad (\text{S16})$$

Now we can make an ODE for dx and dy . Additionally we will include the inertial lift velocity which acts on dy .

$$\dot{dx} \sim dU \quad (\text{S17})$$

$$\dot{dy} \sim dV + \Gamma dy \quad (\text{S18})$$

Now using the experimental values for h and a , along with γ_y , δ_{yy} , and Γ , we can solve this system of ODEs numerically.

CROSS-STREAM EDDIES IN THE ASYMPTOTIC MODEL

Here we show the cross-stream eddies appear in the asymptotic expansion of the flow around a single inertially-focused particle. We consider a channel with dimensions: $H = 35\mu\text{m}$, $W = 60\mu\text{m}$, $AR = 1.7$, and $\alpha = 0.17$.

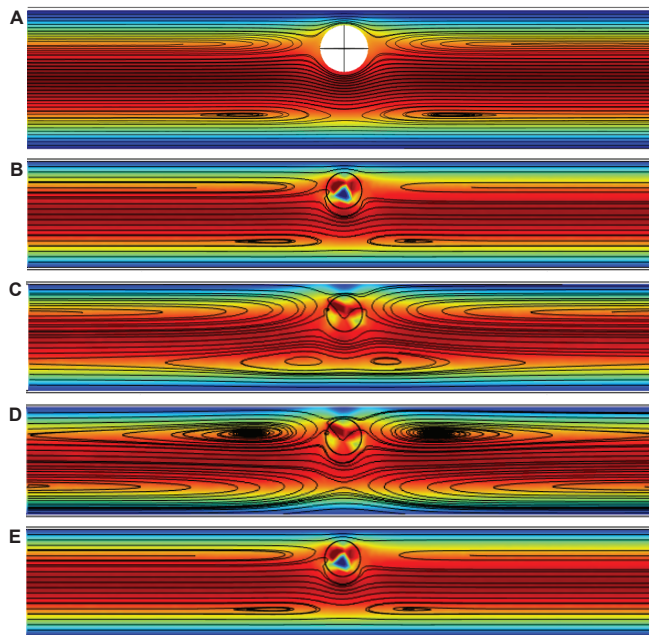


FIG. S2. Fluid streamlines around a single particle in its equilibrium position for (A) the full NSE solution \mathbf{u} , (B) the stresslet \mathbf{v}^{ST} (C) the stresslet plus the first image $\mathbf{v}^{ST} + \mathbf{v}_1$ (D) the stresslet plus two images $\mathbf{v}^{ST} + \mathbf{v}_1 + \mathbf{v}_2$, and (E) the stresslet plus the full computational image $\mathbf{v}^{ST} + \mathbf{v}_\infty$.

Let \mathbf{u} solve the full NSE with exact boundary conditions. We solve for \mathbf{u} numerically using finite element methods in Comsol Multiphysics (Los Angeles, CA). We validate this numerical method in Section .

In the channel, the closest wall to the inertially focused particle is at $y = +H/2$. Recall that \mathbf{v}^{ST} is the stresslet, shown in equation (S4). Let \mathbf{v}_1 , \mathbf{v}_2 and \mathbf{v}_∞ all solve the Stokes equations and satisfies the following boundary conditions:

$$\mathbf{v}_1 = -\mathbf{v}^{ST} \text{ on } y = +H/2, \quad (\text{S19})$$

$$\mathbf{v}_2 = -\mathbf{v}_1 \text{ on } y = -H/2, \quad (\text{S20})$$

$$\mathbf{v}_\infty = -\mathbf{v}^{ST} \text{ on all the channel walls.} \quad (\text{S21})$$

Note that

$$\mathbf{u} = \mathbf{v}^{ST} + \mathbf{v}_\infty + \dots, \quad \text{and} \quad \mathbf{v}_\infty \sim \mathbf{v}_1 + \mathbf{v}_2 + \dots \quad (\text{S22})$$

We plot the streamlines for \mathbf{u} , \mathbf{v}^{ST} , \mathbf{v}_1 , \mathbf{v}_2 , and \mathbf{v}_∞ in Figure S2. Note that the cross stream eddies in \mathbf{u} only appear in $\mathbf{v}^{ST} + \mathbf{v}_1$ and $\mathbf{v}^{ST} + \mathbf{v}_\infty$ (Figure S2 A,C,E). The cross-stream eddies appear after reflecting across the wall at $y = -H/2$. By construction, we have demonstrated that the cross-stream eddies can be quantitatively reproduced using the same model we develop for same streamline interactions, i.e. viscous particle interactions with the wall.

VALIDATING THE NUMERICAL SOLVER AGAINST DATA

To test the accuracy of our numerical solver, we compare to experimental measurements of the drag coefficient of a sphere in a square channel. Chow *et al.* observed the drag coefficient of a sphere whose diameter d is very close to the width W of a square channel [S22]. For this comparison, we use their measurements for the size ratio $d/W = 0.886 \pm 0.008$. The Reynolds number of the flow was defined by $Re = UW/\nu$, where U is the average fluid velocity in an empty channel and ν is the kinematic viscosity of water.

Our numerical solver modeled a square channel with lengths scaled by the channel width W . That is, the square channel had dimensions $1 \times 1 \times 6$, and the particle had radius $a = 0.443$. We used Comsol Multiphysics (Los Angeles, CA) to solve the PDE with variable Reynolds numbers. The particle velocity U_p was chosen arbitrarily to be $U_p = .75U$. We measured the drag force F_D on the particle using Lagrange multipliers. Then the drag coefficient was computed by:

$$C_D = \frac{2F_D}{\pi a^2(U_p - U)^2}. \quad (\text{S23})$$

The results from our numerical solver compare well with the data from Chow *et al.* [S22], especially for $Re \leq 300$ (Figure S3). The range of Reynolds numbers from experiments is $30 \leq Re \leq 110$, which is well within the numerical range of accuracy.

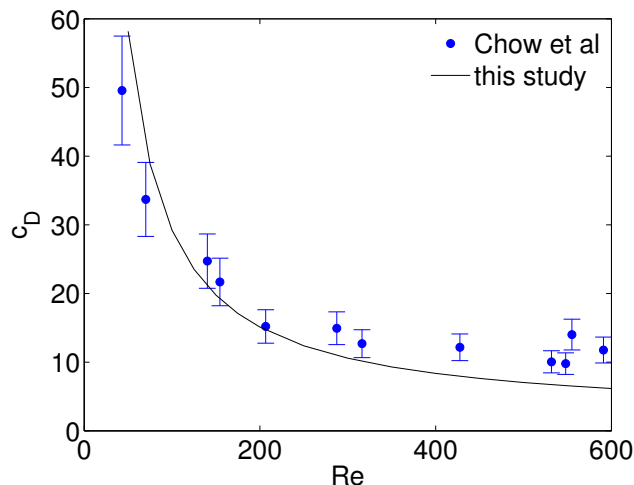


FIG. S3. Drag coefficient dependence on Reynolds number. The results from our numerical solver compare well with the data from Chow *et al.* [S22]